Vibrational Mode Effects as a Probe of Inter-channel Coupling in the Reactions of Formaldehyde Cation with Ammonia and Water†

Jianbo Liu, Brady Uselman, Brian Van Devener, and Scott L. Anderson*

Department of Chemistry, 315 S 1400 E, Room 2020, University of Utah, Salt Lake City, Utah 84112

Received: May 12, 2004; In Final Form: July 9, 2004

We report the effects of collision energy (E_{col}) and five different H_2CO^+ vibrational modes on reaction of H_2CO^+ with ND_3 and D_2O over the center-of-mass E_{col} range from 0.1 to 2.1 eV. Properties of various complexes and transition states were also examined computationally. For water, the only reaction is proton transfer (PT), going by a direct mechanism over the entire E_{col} range, with a cross section near the collision limit. H_2CO^+ vibrational excitation has no effect on reaction with water. Three product channels are observed in reaction with ammonia. Both proton transfer (PT) and charge transfer (CT) have large cross sections over the entire energy range. Hydrogen abstraction by H_2CO^+ from ammonia (HA) accounts for <2% of the total product signal but is a mechanistically interesting channel. Both PT and HA go by direct mechanisms over most of the E_{col} range, but complex mediation may be important at the lowest energies. All three channels are mode-specifically affected by H_2CO^+ vibrational excitation. Vibration controls total reactivity but has essentially no effect on product branching. Charge transfer during reactant approach appears to have a large effect on subsequent PT and HA reactions.

I. Introduction

Reactions of H_2CO^+ with ammonia and water are important in molecular synthesis in interstellar gas clouds, comets, and planetary atmospheres of reducing compositions[1,2] where non-equilibrium conditions may make vibrational effects important. Previous studies on these two systems were performed at 300 K using the ion cyclotron resonance[3,4] and selected ion flow tube techniques.[5,6] In both systems, the main product channel observed was exothermic proton transfer (PT), and for ammonia, charge transfer (CT) was also significant. Here we report a study of the effects of different H_2CO^+ vibrational modes and collision energy (E_{col}) on the integral and differential cross sections for reactions of $H_2CO^+(\nu^+) + ND_3$ and $H_2CO^+(\nu^+) + D_2O$. The E_{col} and vibrational state dependence of the cross sections gives information about inter-channel competition and insight into the effects of energy, angular momentum, and different types of nuclear motion. Product recoil velocity distributions provide complementary information regarding collision time scale, scattering mechanisms, degree of energy randomization, and exit channel interactions. Quantum chemistry and Rice−Ramsperger−Kassel−Marcus (RRKM) theory calculations were carried out to investigate the structures, energetics, and lifetimes of important intermediates and transition states, providing additional insight into the reaction mechanism.

Because ammonia and water are isoelectronic, with similar dipole moments and polarizabilities, and with electron lone pairs available as hydrogen bond acceptors, similarities are expected in the chemistry. The major difference is that the charge transfer (CT) channel is energetically accessible for ammonia, but not for water. As we will show, the opening of the CT channel affects not only product branching, but also the mechanism for other reaction channels.

II. Experimental and Computational Details

The guided ion beam tandem mass spectrometer used in this study has been described previously,[7−10] along with the operation, calibration, and data analysis procedures. The H_2CO precursor was generated by heating a mixture of paraformaldehyde (Aldrich 95%) and anhydrous $MgSO_4$ (Merck) to 60 °C,[11] and sweeping the resulting H_2CO into a pulsed molecular beam valve using a flow of helium at ∼1 atm, giving a H_2CO concentration of ∼5%.[12] H_2CO^+ can be generated in selected vibrational states by REMPI through the $^1A_2(3p_x)$ Rydberg state.[13] For this study, H_2CO^+ was generated in its ground state, or with one quantum in one of the following vibrational modes: ν_2^+ (CO stretch, 0.208 eV), ν_3^+ (CH_2 scissors, 0.143 eV), ν_4^+ (CH_2 out-of-plane bend, 0.114 eV), ν_5^+ (CH_2 asymmetric stretch, 0.337 eV), and ν_6^+ (CH_2 rock, 0.101 eV). Under even low intensity REMPI conditions, the ground electronic state H_2CO^+ is readily photodissociated to HCO^+ and CO^+. To remove these fragment ions from the beam, the ions were generated inside a short radio frequency (rf) quadrupole ion guide, which focused the ions through a pair of ion lenses into a quadrupole mass filter. Mass-selected ions were collected and collimated by a lens set equipped with variable apertures, and a lens that was used to time-gate the ion pulse. The combination of controlled collection radius and time-gating allows us to produce a mass-selected beam with narrow kinetic energy spread ($\Delta E = 0.1$ eV).

The mass-selected, vibrational state-selected, and kinetic energy-selected primary beam was injected into a system of 8-pole rf ion guides.[14] In the first segment of the guide, ions pass through a 10 cm long scattering cell, containing ND_3 or D_2O at 2.0×10^{-5} Torr. ND_3 (Cambridge Isotope Lab, D 99%) gas was used without further purification, and D_2O (Cambridge Isotope Lab, D 99.9%) was purified by freeze−pump−thaw cycles before each experiment. The inlet valve was kept at about 70 °C to avoid freezing ND_3 or D_2O in the valve orifice. Product

† Part of the special issue "Tomas Baer Festschrift".

* Corresponding author. E-mail: anderson@chem.utah.edu.

10.1021/jp040352i CCC: $27.50 © 2004 American Chemical Society
Published on Web 08/26/2004

ions and unreacted primary ions were collected by the ion guide, passed into a second, longer guide segment for time-of-flight (TOF) analysis, then mass analyzed, and counted. Integral cross sections were calculated from the ratio of reactant and product ion intensities, and the calibrated target gas pressure−length product. TOF was used to measure the reactant ion beam velocity distribution (and thus the E_{col} distribution) at each nominal E_{col}, and also to measure the product ion axial velocity distributions discussed below.

For each reactant state we cycled through the series of E_{col} values several times, to minimize systematic error from drifting potentials, etc. As a check on reproducibility, we measured the cross sections for the ground state, both at the beginning and end of each complete experimental run. Finally, the entire set of experiments was repeated several times over a one month period. On the basis of the reproducibility of the cross section measurements, we estimate that the relative error (e.g., uncertainty in comparing data for different vibrational states or E_{col}) is less than 10%. The uncertainty in the absolute scale of the cross section is also estimated to be ~10%, primarily resulting from uncertainties in target pressure and collection efficiency for slow product ions.

Quantum chemistry calculations were performed at the B3LYP/6-311++G** level of theory, using GAUSSIAN03.[15] Geometries were optimized by calculating the force constants at every point. The vibrational frequencies and zero-point energies were scaled by a factor of 0.9613 and 0.9804, respectively.[16] All transition states (TS) were verified to be first-order saddle points by frequency calculations. For comparison, we also performed calculations at the G3 level of the theory. RRKM calculations were done with the program of Zhu and Hase,[17] using its direct state count option, and frequencies and energetics from the B3LYP/6-311++G** calculations.

III. Results and Analysis

A. Integral Cross Sections. The $H_2CO^+ + ND_3$ and $H_2CO^+ + D_2O$ isotope combinations were used in the experiments to look for possible atom scrambling during reactions. For $H_2CO^+ + ND_3$, product ions are observed at mass 20, 21, and 32, corresponding to ND_3^+ (CT), ND_3H^+ (PT), and H_2COD^+ (hydrogen abstraction, HA). In principle, the *m*/*z* 20 and 32 could be $ND_2H_2^+$ and D_2CO^+, from H/D exchange; however, several observations indicate that H/D exchange is not significant in our experiments. If D_2CO^+ were a significant product, we would also expect substantial signal for $HDCO^+$, which is not observed. Similarly, H/D exchange would lead CT products such as ND_2H^+, which are not observed. As will be shown below, the time scale for reactions in these systems is quite short—apparently too short for the rearrangements needed in H/D exchange.

The energetics of the three product channels are as follows:[18,19]

$$H_2CO^+ + ND_3 \rightarrow ND_3^+ + H_2CO \quad \text{CT} \quad \Delta H = -0.72 \text{ eV} \quad (1)$$

$$\rightarrow ND_3H^+ + HCO \quad \text{PT} \quad \Delta H = -2.28 \text{ eV} \quad (2)$$

$$\rightarrow H_2COD^+ + ND_2 \quad \text{HA} \quad \Delta H = 0.13 \text{ eV} \quad (3)$$

One problem in studying this system is that the ND_3^+ and ND_3H^+ products have low velocities in the lab frame. These slow ions have rates[20] near the collision rate for secondary reactions with ND_3:[18,19]

$$ND_3^+ + ND_3 \rightarrow ND_4^+ + ND_2$$

(secondary HA of the CT product) $\Delta H = -0.72$ eV (4)

$$ND_3H^+ + ND_3 \rightarrow ND_4^+ + ND_2H$$

(secondary PT of the PT product) $\Delta H = 0.0$ eV (5)

The reported CT and PT integral cross sections were corrected for these secondary reactions by taking measurements at several ND_3 pressures ranging from 1.0×10^{-4} to 2.0×10^{-5} Torr, then extrapolating to zero ND_3 pressure.

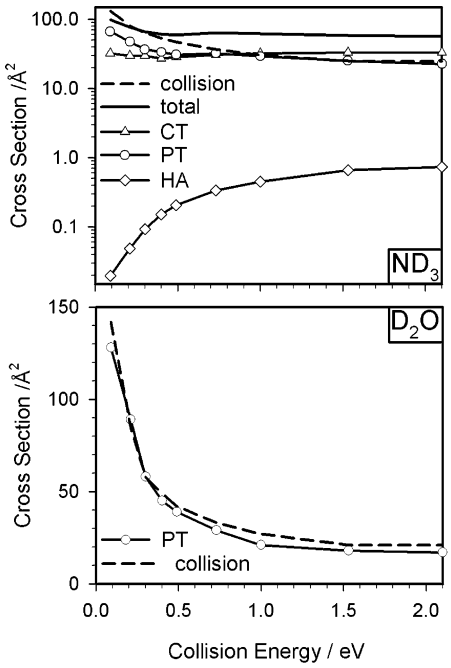

Figure 1. Cross sections for the reaction of ground-state H_2CO^+ with ND_3 (top frame) and D_2O (bottom frame), obtained by linear extrapolation to zero ND_3 and D_2O pressure. Also shown are the estimated collision cross section and the total reaction cross section.

The integral cross sections for reaction of ground-state H_2CO^+ with ND_3 are shown in the top frame of Figure 1 over the E_{col} range from 0.1 to 2.1 eV, in the CM frame. Also shown in the figure are the experimental total cross section (σ_{total} = sum of individual cross section) and an estimate of the collision cross section ($\sigma_{collision}$), taken as the greater of the capture cross section[21] (for $E_{col} \leq 1$ eV) and the hard sphere cross section ($E_{col} > 1$ eV). $\sigma_{HardSphere}$ was calculated as $\pi R_{HardSphere}^2$, where $R_{HardSphere}$ (2.8 Å) is the orientation-averaged center-of-mass contact separation of H_2CO^+ and ND_3, assuming covalent radii for each atom. The dominant channel at low collision energies is PT. The PT efficiency ($=\sigma_{PT}/\sigma_{collision}$) is 50−60% at low energies, approaching 100% at high energies. The CT efficiency ($=\sigma_{CT}/\sigma_{collision}$) increases from 30% at low E_{col} to a nearly E_{col}-independent 130% at high E_{col}. The fact that the CT cross section exceeds the collision limit for $E_{col} \geq 1.0$ eV, indicates that CT can take place at long range, i.e., at inter-reactant separations larger than $R_{HardSphere}$. As a consequence, σ_{total} exceeds $\sigma_{collision}$ except at the lowest collision energies. The endoergic HA cross section shows the expected threshold behavior and accounts for <2% of σ_{total} at all collision energies. The fact that the HA

appearance energy is somewhat lower than the thermodynamical threshold simply reflects our estimated ~0.1 eV E_{col} spread (see below).

For the reaction of H_2CO^+ with D_2O, product ions are observed only at m/z 21, corresponding to D_2OH^+ (PT):[18,19]

$$H_2CO^+ + D_2O \rightarrow D_2OH^+ + HCO \qquad \text{PT}$$
$$\Delta H = -0.65 \text{ eV} \quad (6)$$

As with ND_3, the D_2OH^+ product is slow in the lab frame, and some undergoes secondary reaction with D_2O to produce D_3O^+. Again, we report a cross section corrected by extrapolation to zero D_2O pressure. The corrected cross section for reaction of ground-state H_2CO^+ is shown in the bottom frame of Figure 1, together with the collision cross section estimated as in the case of ND_3. Comparison of σ_{PT} and $\sigma_{collision}$ indicates that the PT reaction efficiency is unity over the entire E_{col} range, within the combined uncertainties of the experiment and collision cross section estimation.

When PT is compared with D_2O and ND_3 in the discussion, we will differentiate them by including the reactant formula in the acronym, e.g., PT(D_2O), where necessary for clarity. The HA and CT channels are understood to be for ND_3, only.

B. Computational Results. H_2CO^+ has a *trans*-$HCOH^+$ isomer, calculated to be ~0.32 eV above H_2CO^+ with a ~1.9 eV barrier to isomerization in the isolated ion.[10] Calculations of Coitino et al.[22] suggests that the barrier is not significantly reduced by complexation to water; therefore we conclude that *trans*-$HCOH^+$ is unlikely to participate in our experiments. Furthermore, most pathways that might generate $HCOH^+$ in reaction with ND_3 and D_2O would likely result in H/D exchange, and no such products were observed.

The computational results for $H_2CO^+ + NH_3$ are summarized in Figure 2 and Table 1. Energetics are reported for all-H species to allow comparison with the literature; however, the calculated energy differences for the appropriate deuterated species are always below 0.1 eV, i.e., within the computational uncertainty. Vibrational frequencies used in the RRKM calculations are those for the D-containing species. Both B3LYP and G3 results are reasonable agreement with experiment, the exception being that the endoergic HA reaction is calculated to be slightly exoergic at the G3 level. There are two isomers for the HA product with hydroxymethyl (H_2COH^+) and methoxy (CH_3O^+) structures. In accord with the thermochemical literature[19] and earlier ab initio work,[23,24] the singlet H_2COH^+ structure is the most stable, giving $\Delta_r H = 0.13$ eV for the HA reaction. Optimizations started in singlet CH_3O^+ geometry converge to H_2COH^+, whereas triplet CH_3O^+ is ~3.5 eV higher than singlet H_2COH^+. Over our energy range, therefore, singlet H_2COH^+ is the only energetically accessible HA product.

Three reactant-like complexes (A−C) and two product-like complexes (D−E) were found with CH_5NO^+ stoichiometry, as shown in Figure 2. In addition, there are other strongly bound species with CH_5NO^+ stoichiometry ($[CH_3ONH_2]^+$, $[CH_2OHNH_2]^+$, $[CH_3NH_2O]^+$, and $[CH_2NH_2OH]^+$) that were studied computationally by Burgers et al.[25] within the context of a general study of the CH_5NO^+ potential energy surface. These complexes are not considered here, because their formation involves either activation barriers inconsistent with the experimental energy dependence, or substantial rearrangements that would almost certainly result in H/D exchange, inconsistent with our observations.

Complexes A, B, and C can be characterized as, respectively, hydrogen-bonded, electrostatic, and σ-bonded; nonetheless, they all have binding energies with respect to reactants of 1.8−2.0 eV. Both Mulliken charge analysis and natural population analysis (NBO) indicate that in complexes A and B, the charge is mostly transferred to the ND_3 moiety, and these complexes are, thus, product-like from the perspective of CT. The charge is roughly equally split in complex C, and presumably it also can decay directly to CT products. Because both complexes A and B are structurally reactant-like, it is unlikely that there would be significant barriers inhibiting their formation. An energy barrier is also unlikely for production of complex C; however, both moieties are significantly distorted, and it is likely that complex C formation is not as facile as formation of A or B. Complexes D and E can be characterized as similar to the PT and HA products, respectively.

Also shown in Figure 2 are possible reaction paths. Observation of a CT cross section in excess of $\sigma_{collision}$ indicates that

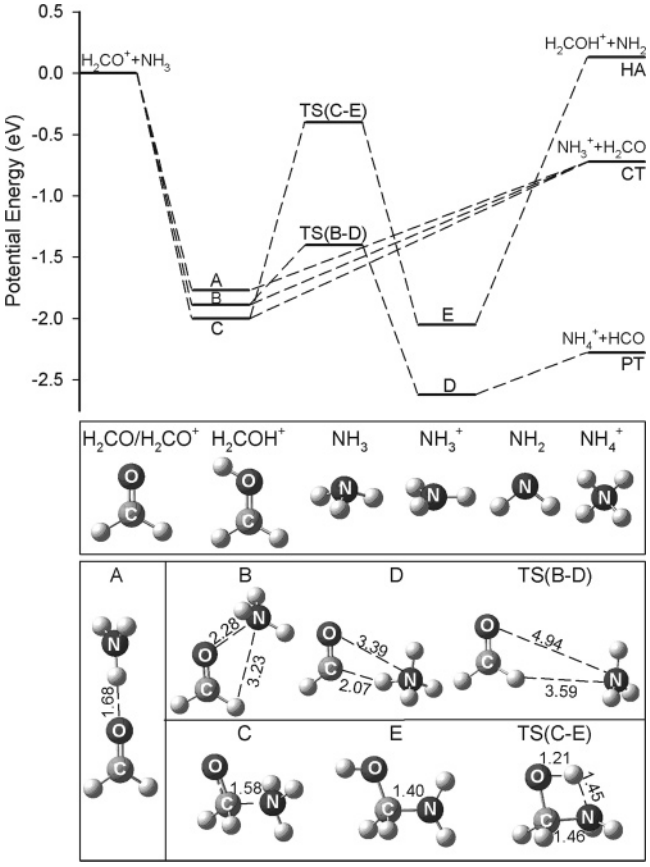

Figure 2. Schematic reaction coordinate for $H_2CO^+ + NH_3$. Energies are derived from a combination of experimental and B3LYP/6-311++G** calculations including zero point energies.

TABLE 1: Experimental and Calculated Energies (eV) Relative to Reactants ($H_2CO^+ + NH_3$)

reaction energetics	B3LYP/6-311++G**[a]	G3(0K)	experimental[b]
$\rightarrow NH_4^+ + HCO$	−2.27	−2.33	−2.28
$\rightarrow NH_3^+ + H_2CO$	−0.67	−0.78	−0.72
$\rightarrow H_2COH^+ + NH_2$	0.08	−0.05	0.13
$\rightarrow CH_3O^+ + NH_2$	3.20	3.55	3.66
complex A	−1.77		
complex B	−1.89		
complex C	−2.00		
complex D	−2.62		
complex E	−2.05		
TS(B−D)	−1.40		
TS(C−E)	−0.40		

[a] Including zero point energy calculated at B3LYP/6-311++G** and scaled by 0.9804. [b] References 18 and 19.

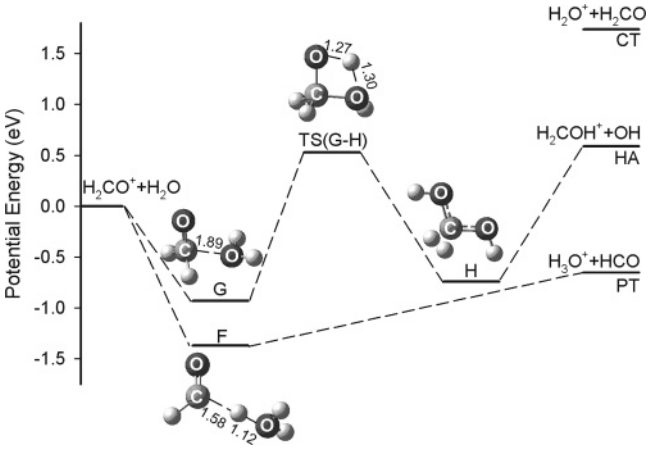

Figure 3. Schematic reaction coordinate for $H_2CO^+ + H_2O$. Energies are derived from a combination of experimental and B3LYP/6-311++G** calculations including zero point energies.

TABLE 2: Experimental and Calculated Energies (eV) Relative to Reactants ($H_2CO^+ + H_2O$)

reaction energetics	B3LYP/6-311++G**[a]	G3(0K)	experimental[b]
$\rightarrow H_3O^+ + HCO$	−0.56	−0.61	−0.65
$\rightarrow H_2O^+ + H_2CO$	1.78	1.67	1.74
$\rightarrow H_2COH^+ + OH$	0.52	0.45	0.59
$\rightarrow CH_3O^+ + OH$	3.64	4.05	4.12
complex F	−1.37		
complex G	−0.93		
complex H	−0.74		
TS(G−H)	0.53		

[a] Including zero point energy calculated at B3LYP/6-311++G** and scaled by 0.9804. [b] References 18 and 19.

CT must be possible in most reactant orientations; i.e., complexes A−C may mediate CT, but complex formation is certainly not required. The lowest energy route found to PT products is reactants → complex B → TS(B−D) → complex D → PT products, although the observed near-unit PT efficiency indicates that, at least for high E_{col}, PT must also occur over a wide range of reactant geometries. The minimum energy pathway to HA products is reactants → complex C → TS(C−E) → complex E → products, and in this case, the vibrational effects provide evidence that this pathway is important, at least for low E_{col}. We were unsuccessful at locating a TS for isomerization of complex A to B, but a relaxed potential energy surface (PES) scan from complex A to B suggests a barrier of <0.56 eV with respect to complex A (1.21 eV below reactants). Given the available energies in our experiments, interconversion between A and B, and possibly C, should be facile, even at low E_{col}.

Computational results for $H_2CO^+ + H_2O$ are summarized in Figure 3 and Table 2. Results at the B3LYP/6-311++G** level are in good agreement with an MP2 study of complexes in $H_2CO^+-H_2O$ by Coitino et al.[22,26] Three complexes (F−H) with $CH_4O_2^+$ stoichiometry were found that might be important in mediating reaction. Complex F is a product-like hydrogen-bonded structure, analogous to complex D for $H_2CO^+ + NH_3$. Attempts to optimize reactant-like complexes analogous to complexes A and B in Figure 2, converged to complex F, indicating a barrierless pathway for PT to water. The reactant-like complex G is analogous to the sigma-bonded complex C for $H_2CO^+ + NH_3$; however, its lower stability and longer inter-moiety bond suggest that the bonding is merely electrostatic. The minimum energy path leading to HA is reactants → complex G → TS(G−H) → complex H → $H_2COH^+ + OH$, analogous to the HA pathway found for $H_2CO^+ + NH_3$. The energy of both the barrier TS(G−H) and products is substantially higher in the water reaction, presumably accounting for the absence of HA products. The most important difference between the water and ammonia energetics is that the CT channel is 1.74 eV endoergic. As a result, CT products are not observed, and it is also unlikely that significant mixing of the $H_2CO^+ + H_2O$ and $H_2CO + H_2O^+$ charge states occurs during collisions.

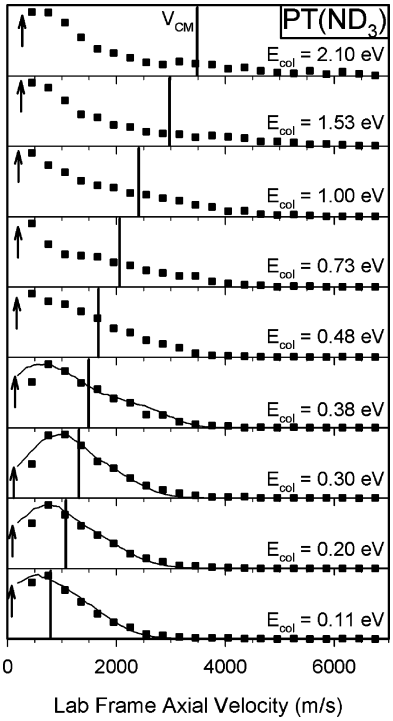

Figure 4. Axial recoil velocity distributions for the PT channel of $H_2CO^+ + ND_3$. Solid symbols: experimental. Solid line: simulation based on the osculating complex model. Heavy vertical line: $\langle V_{CM} \rangle$. Arrow: spectator stripping limit product velocity.

C. Recoil Velocity Distributions. Axial velocity (v_{axial}) distributions are simply the projection of the full velocity distributions on the ion guide axis. The lab frame v_{axial} distributions for PT(ND_3), CT(ND_3), HA(ND_3), and PT(D_2O) product ions are given in Figures 4−7, respectively. Also shown as solid vertical lines in each figure are the velocities of the CM frame with respect to the lab frame, $\langle V_{CM} \rangle$, averaged over the reactant ion beam velocity spread and target thermal motion. Because our experiments are symmetric about the guide axis, the lab frame v_{axial} distributions can be approximately converted to the CM frame simply by subtracting $\langle V_{CM} \rangle$. The raw lab-frame v_{axial} distributions, thus, provide useful insight into the scattering dynamics. For example, if reaction is mediated by a complex with lifetime ($\tau_{collision}$) greater than its rotational period ($\tau_{rotation}$), the resulting v_{axial} distribution must be symmetric about $\langle V_{CM} \rangle$. Conversely, an asymmetric v_{axial} distribution is a clear sign that reaction is direct (i.e., not complex-mediated), and also reveals the predominant scattering mechanism (i.e., forward vs backward scattering). In addition, the deviation of the velocity distribution from $\langle V_{CM} \rangle$ is a measure of the energy going into recoil.

There are a few limitations of this technique, as implemented here. Product ions that are strongly backscattered in the CM frame may have negative laboratory velocities. To collect such ions, the lens at the entrance end of the ion guide is biased positive relative to the guide potential, thus reflecting these ions

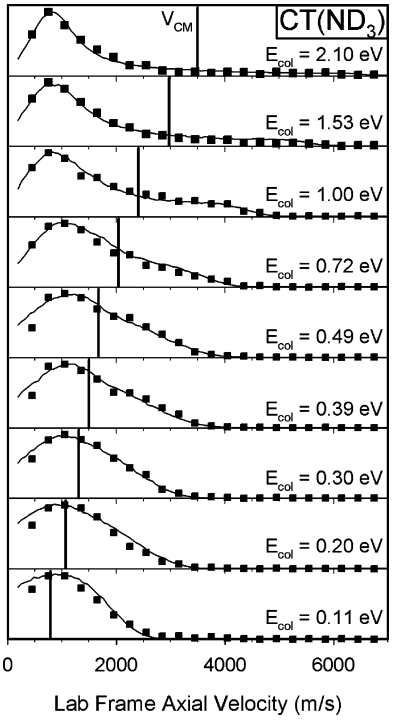

Figure 5. Axial recoil velocity distributions for the CT channel of $H_2CO^+ + ND_3$. Solid symbols: experimental. Solid line: simulation based on the osculating complex model. Heavy vertical line: $\langle V_{CM} \rangle$.

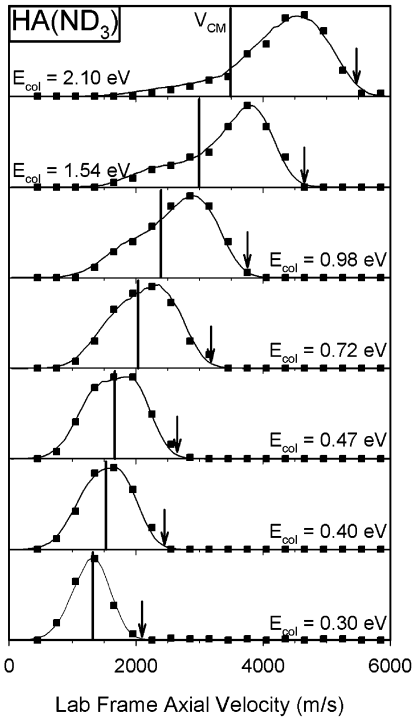

Figure 6. Axial recoil velocity distributions for the HA channel of $H_2CO^+ + ND_3$. Solid symbols: experimental. Solid line: simulation based on the osculating complex model. Heavy vertical line: $\langle V_{CM} \rangle$. Arrow: spectator stripping limit product velocity.

back toward the detector. The reflected ions appear at long flight times, corresponding to low but positive lab velocities. In addition, the slowest ions are most likely to undergo secondary reactions, and to have their velocities distorted by small inhomogeneities in the surface potentials on the ion guides. Finally, these distortions in the low velocity portion of the v_{axial} distributions are exacerbated by the singular TOF-to-velocity

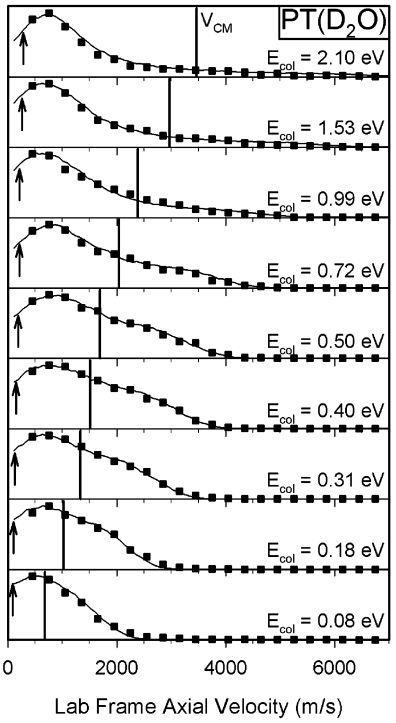

Figure 7. Axial recoil velocity distributions for the PT channel of $H_2CO^+ + D_2O$. Solid symbols: experimental. Solid line: simulation based on the osculating complex model. Heavy vertical line: $\langle V_{CM} \rangle$. Arrow: spectator stripping limit product velocity.

Jacobian. The problem appears to be significant for the PT(ND_3), PT(D_2O) and CT(ND_3) channels, as they produce the slowest product ions. In fitting the velocity distributions, data points at velocities below 450 m/s, where the distortions are most problematic, are omitted.

At high E_{col}, the velocity distributions for PT(ND_3), CT(ND_3), and PT(D_2O), are all peaked well backward of (slower than) $\langle V_{CM} \rangle$, whereas the distributions for HA(ND_3) are forward-peaked. Note that we define scattering angle in terms of product *ion* velocity relative to that for the reactant ion. For all ND_3 and D_2O reactions at high E_{col}, therefore, the velocity peaks correspond to reaction mechanisms wherein the electron or atom transfer events are not accompanied by large momentum transfer, i.e., to small angle scattering. All channels at high E_{col}, therefore, are dominated by large impact parameter collisions, although the presence of tails in the v_{axial} distributions extending well into the forward (PT and CT) or backward (HA) directions indicates that more intimate collisions also contribute, leading to rebounding product ions. For comparison, the velocities expected from a spectator-stripping mechanism[27] are indicated with arrows in Figure 4, 6, and 7. Note that the v_{axial} peaks for PT(ND_3) and PT(D_2O) at high E_{col} approach the spectator limit but that the HA reaction continues to peak well below the spectator-limit velocity.

For CT, the v_{axial} distributions at high E_{col} peak near 800 m/s. This peak velocity must be interpreted with some caution because of uncertainties in velocity measurements for slow ions. It might be, for example, that the true peak is at lower velocities, with the apparent peak at ~800 m/s merely an artifact of declining detection efficiency for slower ions. If that were the case, then we should see similar peak velocities for the PT(ND_3) channel (Figure 4), where similar kinematics imply similar velocity artifacts. Because the high E_{col} PT(ND_3) distributions show no sign of dropping off at low velocities,

we conclude that the CT distributions really do peak significantly above zero lab velocity.

As E_{col} is decreased, v_{axial} distributions for CT(ND_3), PT(ND_3), and PT(D_2O) become less backward peaked, possibly becoming forward−backward symmetric at our lowest E_{col}. At this energy, however, V_{CM} approaches the limit of reliable v_{axial} measurement, so that we essentially only measure the high velocity half of the distributions. On the other hand, the distribution for HA(ND_3) clearly becomes forward−backward symmetric by $E_{col} = 0.3$ eV, where we are still able to record the entire distribution. The transition to (or toward) forward−backward symmetry is consistent with a mechanism where the collision time increases with decreasing E_{col}, approaching $\tau_{rotation}$ at the lowest energies. The osculating complex model[28] was developed to describe velocity distributions in just such situations, thus we have used this model to simulate/fit the recoil velocity distributions. Fitting allows us to extract somewhat more quantitative insight from the distributions, by accounting for experimental broadening resulting from the angular and velocity distributions of both reactants. Our fitting program and procedures have been described previously.[7] In the osculating complex model, a short-lived collision complex forms, with rotational angular momentum equal to the orbital angular momentum of the collision. The rotating collision complex is assumed to decay to products with a lifetime, $\tau_{complex}$, and recoil energy distribution, $P(E_{recoil})$. Here $P(E_{recoil})$ is assumed to be a Gaussian distribution controlled by width and peak-value parameters defined in terms of the available energy in each product channel. The degree of forward−backward symmetry in the distribution depends only on the ratio of $\tau_{collision}/\tau_{rotation}$. To put $\tau_{collision}$ on an absolute basis, $\tau_{rotation}$ can be estimated from the moment of intertia for the collision complex and the available angular momentum, estimated in turn, from the magnitude of the cross section and E_{col}. Assuming a complex like A in Figure 2, forming with a cross section at the capture limit, $\tau_{rotation}$ drops smoothly from ~1.8 ps at $E_{col} = 0.1$ eV to 0.39 ps at $E_{col} = 2.1$ eV. For the PT(ND_3) channel, simulations were only done for $E_{col} \leq 0.39$ eV, because at higher E_{col} the distributions peak at lab velocities below 450 m/s, where our velocity measurements are unreliable. Lab velocities are also low for the PT(D_2O) and CT(ND_3) channels; however, the peaks are within the experimentally accessible range, so unambiguous fits are possible, at least within the constraints of the osculating complex model.

The solid curves shown in Figures 4−7 are fits to the v_{axial} distributions of product ions based on the osculating complex model, and numerical results are summarized in Tables 3 and 4. Note that $\tau_{collision}$ drops rapidly with increasing E_{col}, indicating that complex-mediated mechanisms can be significant only at low E_{col}. As an indication of the collision time that might be expected in the limit of a direct reaction, the tables also give τ_{fly-by}, taken as the time required for reactants to move a relative distance of 5C. In the osculating complex model, the degree of forward−backward symmetry is assumed to result entirely from rotation of the collision complex, and this assumption is probably only reasonable in this system at low E_{col}. For high energies, where $\tau_{complex}$ is negligible, the shape of the v_{axial} distributions is more a measure of the distribution of impact parameters contributing to each product channel. We are also able to extract an estimate of the average energy partitioned into recoil, $\langle E_{recoil} \rangle$. For all but the HA channel, the $\langle E_{recoil} \rangle$ values extracted should be lower limits on the true values, because ions with low lab velocities (i.e., high CM velocities) are excluded from the fits. The tables give both $\langle E_{recoil} \rangle$ and the fraction of E_{avail} going into recoil ($\langle E_{recoil} \rangle / \langle E_{avail} \rangle$). For all channels, both $\langle E_{recoil} \rangle$ and $\langle E_{recoil} \rangle / \langle E_{avail} \rangle$ increase with increasing E_{col}, consistent with faster collisions not allowing for energy redistribution.

TABLE 3: Product Ion Velocity Distribution Fit Results for $H_2CO^+ + ND_3$

E_{col} (eV)	$\langle E_{avail} \rangle^a$ (eV)	$\langle E_{recoil} \rangle$ (eV)	$\langle E_{recoil} \rangle / \langle E_{avail} \rangle$ (%)	$\tau_{collision}$ (ps)	$\tau_{fly-by}{}^b$ (ps)
			ND_3H^+ (PT)		
0.11	2.45	0.24	10	0.88	0.38
0.20	2.54	0.24	9	0.48	0.28
0.30	2.67	0.21	8	0.36	0.23
0.39	2.76	0.33	12	0.21	0.20
			ND_3^+ (CT)		
0.11	0.89	0.20	22	1.8	0.38
0.20	0.98	0.27	28	1.3	0.28
0.30	1.08	0.25	23	0.92	0.23
0.39	1.17	0.28	24	0.41	0.20
0.49	1.27	0.31	24	0.33	0.18
0.72	1.50	0.35	23	0.18	0.15
1.00	1.77	0.59	33	0.11	0.12
1.53	2.31	1.01	44	< 0.10	0.10
2.10	2.89	1.43	49	< 0.10	0.09
			H_2COD^+ (HA)		
0.30	0.22	0.05	0.23	0.36	0.23
0.40	0.34	0.11	0.32	0.33	0.20
0.47	0.41	0.14	0.34	0.32	0.18
0.72	0.65	0.20	0.31	0.14	0.15
0.98	0.91	0.32	0.35	< 0.10	0.13
1.54	1.47	0.51	0.35	< 0.10	0.10
2.10	2.03	0.84	0.41	< 0.10	0.09

[a] $\langle\ \rangle$ = mean value. [b] τ_{fly-by} defined as time for undeflected reactants to travel a relative distance of 5.0 Å.

TABLE 4: Product Ion Velocity Distribution Fit Results for PT of $H_2CO^+ + D_2O$

E_{col} (eV)	$\langle E_{avail} \rangle^a$ (eV)	$\langle E_{recoil} \rangle$ (eV)	$\langle E_{recoil} \rangle / \langle E_{avail} \rangle$ (%)	$\tau_{collision}$ (ps)	$\tau_{fly-by}{}^b$ (ps)
0.08	0.79	0.18	23	0.83	0.44
0.18	0.89	0.23	26	0.54	0.29
0.31	1.02	0.32	31	0.33	0.22
0.40	1.11	0.39	35	0.32	0.20
0.50	1.21	0.43	36	0.23	0.18
0.72	1.43	0.55	38	0.15	0.15
0.99	1.70	0.83	49	< 0.1	0.13
1.53	2.24	1.27	57	< 0.1	0.10
2.10	2.80	1.71	61	< 0.1	0.09

[a] $\langle\ \rangle$ = mean value. [b] τ_{fly-by} defined as time for undeflected reactants to travel a relative distance of 5.0 Å.

The v_{axial} distributions for reaction of vibrationally excited H_2CO^+ are qualitatively similar to those shown for ground-state reactants. For the endothermic HA(ND_3) channel, H_2CO^+ vibrational excitation slightly broadens the distribution, presumably reflecting the higher E_{avail} for vibrationally excited reactants. In addition, the distribution is slightly more forward-peaked in the E_{col} range from 0.3 to 0.72 eV, which may reflect either shortened complex lifetimes and/or HA occurring at larger impact parameters. In either case, vibration accelerates the transition from scattering characteristic of low E_{col} to high E_{col} scattering. For the strongly exoergic channels, no significant effects are observed, as expected because the change in E_{avail} is negligible, and recoil distributions largely reflect exit channel dynamics which tend not to be very dependent on reactant state.[29]

D. Vibrational Effects. Figure 8 shows the E_{col} dependence of σ_{HA} for reaction of H_2CO^+ in different vibrational states with ND_3. Figure 9 shows the dependence on vibrational state, of

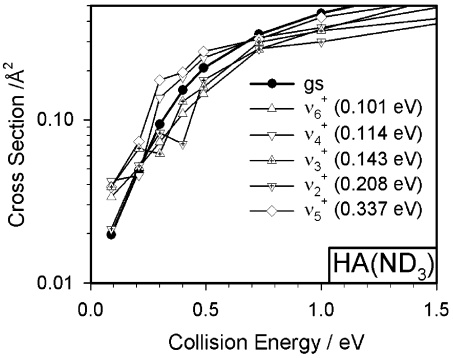

Figure 8. HA reaction cross sections for all H_2CO^+ vibrational states.

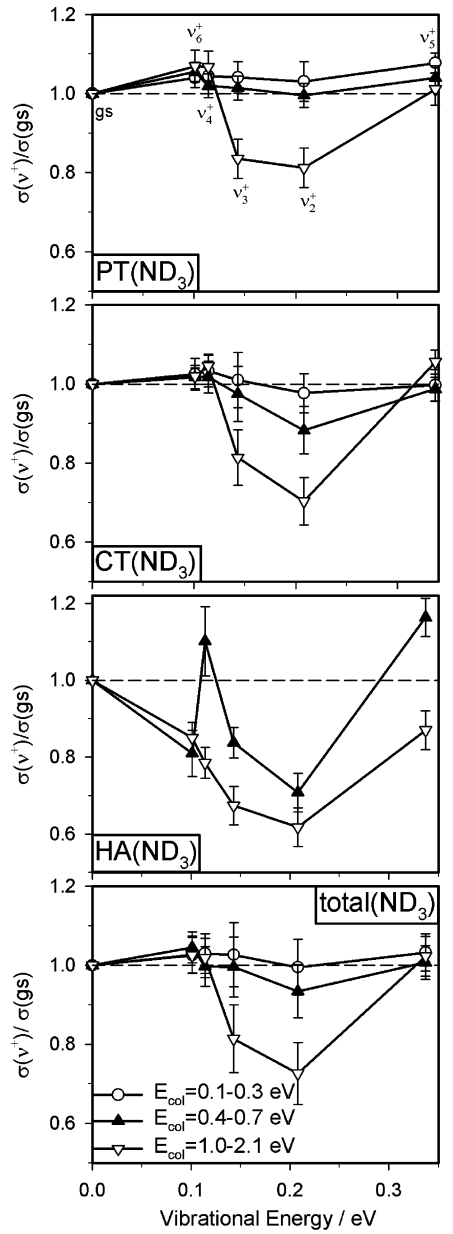

Figure 9. Vibrational enhancement/inhibition factors vs E_{vib}, for different E_{col} range, for the reactions of $H_2CO^+ + ND_3$.

all product channels and the total cross section. The effects are given as vibrational enhancement/inhibition factors, $\sigma(\nu^+)/\sigma$(gs), with each E_{vib} corresponding to one of the six states studied (labels in top frame). To reduce statistical uncertainty in the ratios, data for ranges of E_{col} have been averaged. The error bars were estimated by variations between multiple data sets. Clearly, the effects of H_2CO^+ vibration are quite mode specific, and also strongly dependent on the collision energy. One might expect vibrational effects to be largest at low E_{col}, where E_{vib} makes up a significant fraction of the reactant energy. Here, the largest vibrational effects occur at the highest energies, and only the minor HA channel shows strong vibrational dependence at low E_{col}. In contrast to the vibrational effects on the $H_2CO^+ + ND_3$ system, the reaction with D_2O is independent of H_2CO^+ vibration at all E_{col}; thus no data are shown for that system.

IV. Discussions

A. Charge Transfer. *(1) High Collision Energies.* The CT channel is endoergic for reaction with D_2O, and no CT products are observed. In reaction with ND_3, the CT cross section exceeds the collision cross section at high E_{col} (taken as $\sigma_{HardSphere}$ for $E_{col} > 1.0$ eV). Such a large σ_{CT} implies that CT must be efficient at large inter-reactant separations, so that it occurs for impact parameters (b) larger than $R_{HardSphere}$ (~2.8 Å). Because little momentum transfer can occur in the limit of a long-range electron-transfer mechanism, the product ion velocity should be close to that of the neutral reactant—in this case corresponding to $v_{axial} \approx 0$. Figure 5 shows that the velocity distributions at high E_{col} do, indeed, peak at low v_{axial}, with a weak tail extending well into the forward direction. The tail simply indicates that in addition to the dominant long-range mechanism, CT can occur in small impact parameter collisions, where large momentum transfer occurs. Two factors contribute to the dominance of the long-range mechanism. First, the integral cross section is *b*-weighted, thus long-range mechanisms tend to dominate whenever they occur with reasonable efficiency. In this system, competition with the PT channel is also a factor. Near-unit PT efficiency implies that most collisions where reactants approach close enough to allow atom transfer, must ultimately lead to PT. As a consequence, the observed CT product ions must mostly originate in large *b* collisions.

Several factors are expected to control the efficiency of long-range CT.[30] As noted, little collisional momentum transfer can occur; thus E_{recoil} should be close to E_{col}. As a consequence, the internal energy of the product state must be nearly resonant with the reactant state; i.e., the substantial CT exoergicity must be accommodated as internal energy. Long-range electron transfer is essentially an electronic transition, wherein the orbitals involved happen to be on different molecules. Therefore, in addition to the requirement of near-resonance, CT probability should reflect the Franck−Condon factors connecting initial and final states. This aspect of the mechanism is elaborated below, in the context of vibrational effects on CT.

The 800 m/s v_{axial} peak for CT products at $E_{col} = 2.1$ eV corresponds to a CM frame product recoil energy of only 1.3 eV. This tells us that the most efficiently populated CT product states are actually not near-resonant, but rather have average internal energy ~0.8 eV greater than the CT exoergicity. It is, at first, quite counter-intuitive that so much translation-to-internal energy ($T \rightarrow E_{internal}$) conversion could occur in a long-range collision. The requirement for $T \rightarrow E_{internal}$ conversion should set an upper limit on the average impact parameter leading to CT ($b_{critical}$), and therefore on the CT cross section. As noted, CT must occur mostly in the impact parameter range greater than $b_{HardSphere}$, with PT occurring in most collisions with $b < b_{HardSphere}$. In that case, $b_{critical}$ is related to the *total* cross section by the relation:

$$\sigma_{total} = 2\pi \int_0^{b_{critical}} P(b) b \, db$$

Because it is not clear how $P(b)$ varies with b, we assume that $P(b) = 1$ for $b < b_{critical}$, and $P(b) = 0$, otherwise, so that the resulting $b_{critical}$ value should be considered an effective cutoff impact parameter for CT. At high E_{col}, $\sigma_{total} = 57$ Å^2; therefore, $b_{critical} = 4.25$ Å. In a collision with $b = b_{critical}$, there is some inward deflection that results from the attractive long-range potential. To estimate this deflection, a classical trajectory was calculated for $E_{col} = 2.1$ eV and $b = b_{critical}$, using forces from the ion-induced-dipole and ion−dipole potentials, the latter estimated using the $\cos(\langle\theta\rangle)$ implementation of the average dipole orientation model.[31] The deflection turns out to be ~0.14 Å; thus the closest approach for a collision at $b_{critical}$ is ~4.1 Å, providing an estimate of the maximum distance at which CT occurs with substantial probability (R_{CT}). R_{CT} is, thus, ~50% larger than $R_{HardSphere}$. The final question is whether the inter-reactant forces at this separation are large enough to account for the observed 0.8 eV most probable T → $E_{internal}$ conversion. The most likely mechanism for T → $E_{internal}$ transfer at long range is via the ion−dipole potential, which depends on both the orientation angle and umbrella-bending coordinate of the ND_3 reactant. The corresponding forces couple translation to rotation and ν_2 vibration of ND_3.

To test whether such long-range electrostatic couplings could result in the observed T → $E_{internal}$ transfer, we calculated a few quasi-classical direct-dynamics trajectories at the MP2/6-31G* level of theory, using the updating Hessian method in GAUSSIAN03,[15] with initial conditions generated by the VENUS program of Hase and co-workers.[32] The $H_2CO^+ + ND_3$ system is unsuitable for such calculations because of collisional mixing with the low-lying $ND_3^+ + H_2CO$ state. Instead, we calculated trajectories for $H_2CO^+ + D_2O$, where the kinematics and dipole moment are similar, but the $D_2O^+ + H_2CO$ charge state is high enough in energy that it is unlikely to couple strongly. Clearly the energy transfer dynamics will be somewhat different for D_2O and ND_3; however, the systems are similar enough to allow semiquantitative comparisons. Trajectories were calculated for $E_{col} = 2.1$ eV, and $b = 4.25$ Å—conditions relevant to T → $E_{internal}$ transfer at $b_{critical}$ for $H_2CO^+ + ND_3$. Not surprisingly, the amount and rotation−vibration branching of the T → $E_{internal}$ transfer varies with orientation and vibrational phase in the individual trajectories; however, the rotational energy of the scattered $H_2CO^+ + D_2O$ typically is 0.7−0.9 eV higher than that of the reactants, in good agreement with the 0.8 eV T → $E_{internal}$ transfer observed. The trajectories show some transfer to the D_2O bending coordinate as well; however, vibrational excitation in these quasi-classical trajectories is unlikely to be accurate, due to lack of vibrational quantization. In any case, it is clear that the anisotropic long-range potential can account for the observed level of T → $E_{internal}$ conversion, even in large impact parameter collisions.

(2) Low Collision Energy. As the collision energy is lowered, the CT cross section remains nearly constant. Presumably, the range of impact parameters where CT can occur (i.e., $b_{critical}$) increases with decreasing energy because of increased inward deflections. However, this increase in $b_{critical}$ is offset by a concomitant increase in σ_{PT}; i.e., the increased inward deflection also increases the range of b leading to the competing PT channel. At the lowest collision energies, the PT cross section is only $\sim 0.5\sigma_{collision}$, raising the possibility that CT products may result from small impact parameter collisions, as well as in the long-range collisions where there is no competition from PT. One question, therefore, is whether intermediate complexes are important in mediating CT. Certainly if a complex such as complex A, B, or C (Figure 2) forms in collisions, these can dissociate to CT products, in addition to transforming to other geometries that lead on to HA or PT products. If a complex-mediated mechanism is important in low E_{col} CT, then we should see forward−backward symmetric υ_{axial} distributions; however, we are not able to measure the slow, backscattered ions for low E_{col}. All we can say is that the E_{col} dependence of the υ_{axial} distributions is suggestive of a complex-mediated mechanism at low E_{col}. Consider the distribution at $E_{col} = 1.0$ eV. Note that the cutoff velocities for the forward- and backward-scattered components are symmetric about V_{CM}, precisely as would occur if rotation of a short-lived complex transferred a fraction of the (normally backscattered) product flux to the forward hemisphere. Furthermore, as E_{col} is reduced, the relative intensity of the forward component gradually increases, as would be expected in a complex mechanism, because $\tau_{complex}$ should increase with decreasing energy.

RRKM calculations[17] were performed to see if any of the complexes shown in Figure 2 might account for the collision times inferred from the υ_{axial} fits (Table 3). For each complex, all decomposition channels indicated by dashed lines in Figure 2 were included. For decay of complexes A−C to reactants and CT products, and of complexes D and E to PT and HA products, there are no energy barriers, and we assumed orbiting transition states.[33] For these calculations, we used average angular momenta corresponding to the capture cross section, i.e., $R_{collision} = \mu\upsilon_{rel}(\sigma_{capture}/\pi)^{1/2}$, where μ and υ_{rel} are the reduced mass and relative velocity, respectively. The dominant decay channel for complexes A and C is to CT products, with a lifetime approaching 1 ps at low E_{col}, consistent with $\tau_{collision}$ extracted from the υ_{axial} fits. The RRKM results, thus, suggest that complexes A and C might play a significant role in mediating CT at energies below ~0.5 eV. We note, however, that if these complexes interconvert rapidly with complex B, the very rapid decay of B (see below) would reduce the lifetimes of A and C as well.

B. Proton Transfer. For PT from H_2CO^+ to D_2O, it is unlikely that the excited $H_2CO + D_2O^+$ charge state is important, as it is almost 2 eV above the reactant state. In contrast, the $H_2CO + ND_3^+$ charge state is the ground state of the $(H_2CO + ND_3)^+$ system, and the large CT cross section implies that collisional mixing of the $H_2CO^+ + ND_3$ and $H_2CO + ND_3^+$ states is efficient, even at large inter-reactant separations. Such mixing must also occur in small impact parameter collisions during reactant approach. Given that the charge is largely on the ND_3 moiety in complexes A−C, it seems likely that the actual atom transfer reactions take place in the $H_2CO + ND_3^+$ charge state.

The velocity distributions for PT(ND_3) and PT(D_2O) (Figures 4 and 7) are clearly asymmetric with respect to V_{CM}, except possibly at the lowest E_{col}, where we cannot exclude a symmetric distribution. The υ_{axial} fits suggest that collision times are subpicosecond even at the lowest E_{col} and become comparable to τ_{fly-by} by ~0.5 eV. In the figures, vertical arrows show the product velocity predicted by the spectator-stripping mechanism,[27] expected to be a reasonable model in the limit of direct reaction in impulsive, large-impact parameter collisions. The spectator stripping velocities are in the experimentally inaccessible range for all E_{col}; however, it appears that for PT(D_2O), the distributions peak at higher lab velocities (i.e., lower CM recoil velocities) than predicted by spectator stripping. For PT(ND_3) at high E_{col}, the υ_{axial} distributions are similar to those for PT(D_2O), as might be expected; however, the PT(ND_3) distributions appear to peak at lower lab velocities (i.e., higher CM υ_{recoil}) than those for PT(D_2O) channel, i.e., closer to the

spectator stripping predictions. Higher v_{recoil} and dynamics closer to the stripping limit are reasonable, given that the exoergicity is substantially higher for the ND_3 reaction.

At the lowest E_{col}, the v_{axial} fits do not rule out mediation by a complex with lifetime approaching 1 ps. For $H_2CO^+ + ND_3$, complexes B and D are on the obvious PT reaction path, and their RRKM lifetimes were calculated with respect to the decay pathways shown in Figure 2. Given that it is weakly bound with respect to the large amount of available energy in the PT exit channel, it is not surprising that complex D has a negligible RRKM lifetime with respect to dissociation to PT products. (The calculated lifetime is on the order of a single vibrational period, i.e., too short to treat with RRKM theory.) For complex B, decay back to reactants is on the nanosecond time scale; however, decay over TS(B−D) and then on to PT products is calculated to occur on the <100 fs time scale even at our lowest E_{col}, i.e., shorter than τ_{fly-by}. As noted above, complex A has a non-negligible RRKM lifetime at low E_{col}. If this complex simply dissociates, CT products are the result. If complexes A and B interconvert, this would allow complex A to contribute to the PT products; however, if interconversion is facile, that would also decrease the complex A lifetime substantially. We also calculated lifetimes and decay branching for complex F in the $H_2CO^+ + D_2O$ system. Complex F is found to decay exclusively to PT products, and with lifetimes below 100 fs at all E_{col}. The conclusion is that there are no mechanistically significant complexes along the PT(ND_3) and PT(D_2O) reaction paths over our entire E_{col} range.

As required for transfer of a light atom in a stripping-like mechanisms, the fitted recoil energies are close to E_{col}. The average value $\langle E_{recoil} \rangle$ is ∼82% of E_{col} for $E_{col} > 1$ eV. The implication is that the reaction exoergicity (2.28 eV for PT(ND_3), 0.65 eV for PT(D_2O)) is largely converted to internal energy of the products, rather than appearing as recoil energy. $E_{recoil} \approx E_{col}$ also implies that most of the reactants' collisional angular momentum must go to recoil angular momentum of the products; thus most of the products' internal energy must be in vibration. Given that HCO is bent at an angle close to the HCO angle in H_2CO^+, and that neither the D_2O or ND_3 geometries change substantially when protonated, it is likely that this internal energy is, initially at least, deposited into modes that involve substantial D_3N-H and D_2O-H stretching. Similar energy disposal behavior has been observed for proton transfer in other heavy + light−heavy systems, for example, in theoretical[34−37] and experimental[37] studies of PT in $H_3O^+ + NH_3$.

C. Hydrogen Abstraction. The one channel where the v_{axial} distribution is clearly forward−backward symmetric at low E_{col} is HA. The osculating complex fit at $E_{col} = 0.30$ eV suggests that $\tau_{complex}$ is comparable to $\tau_{rotation}$. To estimate $\tau_{rotation}$, we need some estimate of the range of impact parameters (and thus the range of $R_{collision}$) contributing to this channel. For the PT and CT channels at low E_{col}, it is reasonable to estimate b_{max} from the capture cross section. For HA, it is not clear if the small reaction cross section indicates that reaction occurs with low probability over a wide range of b, or if HA occurs only in a small range of impact parameters. At high E_{col}, the fact that the v_{axial} distributions are strongly forward peaked indicates that HA must be possible in large b collisions, although it is not clear that this is still true at low energies, where complex formation is an issue. Nonetheless, for want of a better method, we have taken b_{max} from the capture limit. With that assumption, the collision times reported in Table 3 are on the order of half a picosecond at low E_{col}.

A reactant-like complex that might contribute to the HA channel is complex A, which has the correct N−H−O bonding arrangement. RRKM theory suggests, however, that complex A decays to almost exclusively to CT products with less than <0.1% branching to HA products. The complex that obviously can decay to HA products is complex E, which also could potentially decay to PT and CT products. We were unable to locate a TS for complex E → PT; however, it is likely to be tight and high in energy, because extensive rearrangement is required. Complex E → CT would be by TS(C−E), followed by dissociation. The RRKM lifetimes of complexes C and E were calculated for decay paths shown in Figure 2 (i.e., complex E → PT products is not included). Complex C decays, mostly to CT products, on a fast time scale (<0.1 ps) at $E_{col} = 0.3$ eV. The branching from complex C to complex E (and on to HA products) decreases with increasing E_{col} because TS(C−E) is tighter than orbiting TSs governing dissociation to reactants or CT products. Complex E overwhelmingly decays to HA products, with a lifetime of >1 ps at $E_{col} < 0.5$ eV, and thus could account for the forward−backward symmetric v_{axial} distributions. As discussed below, the vibrational effects on this channel support a reaction coordinate wherein the H_2CO moiety is out-of-plane bent, consistent with passage through TS(C−E).

HA is clearly direct at high energies, and goes with nearly E_{col}-independent efficiency of 2−3% ($=\sigma_{HA}/\sigma_{collision}$). The strong forward scattering at high E_{col} indicates that HA is dominated by collisions at large impact parameter; however, the continued presence of a small backward scattered velocity component suggests that more central collisions can result in HA by a rebound mechanism. The v_{axial} peak remains well below the velocity predicted by the spectator stripping mechanism at all E_{col} (arrows in Figure 6), unlike the PT(ND_3) and PT(D_2O) channels, which approach stripping behavior at high E_{col}. This presumably reflects the fact that HA requires breaking a much stronger bond than PT, so that higher collision energies would be required to reach the stripping limit ($D_0(D_2N-D) = 4.6$ eV; $D_0(HCO-H^+) = 1.09$ eV).[18]

In the $H_2CO^+ + CD_4$ system the analogous HA reaction is also observed, although in that case, HA is exoergic and is the dominant channel. Despite the difference in energetics, HA in the CD_4 reaction also goes with low (16%) and near-E_{col}-independent efficiency at high E_{col}. In that system, we concluded that the efficiency at high E_{col} must be controlled by collision orientation, even though neither H_2CO^+ nor CD_4 are reactants one would normally associate with strong steric hindrance.[38] Subsequently, we carried out a trajectory study of the reaction, and found that HA occurs only in a very restricted range of reactant orientations, with CD_4 approaching such that the nascent CO-D bond angle is within ∼15° of the ∼116° equilibrium bond angle in the H_2COD^+ product.[39] Because this orientation constraint appears to be dictated by the product geometry, it is not unreasonable to assume that HA in the $H_2CO^+ + ND_3$ system should also be strongly orientation dependent. In $H_2CO^+ + ND_3$, the HA efficiency at high E_{col} is just 2−3%, considerably lower than the 16% efficiency observed for $H_2CO^+ + CD_4$. We propose that for $H_2CO^+ + ND_3$, the HA efficiency is further reduced by competition with the dominant PT and CT channels, neither of which are significant in the $H_2CO^+ + CD_4$ system.

D. Vibration Effects. *(1) Vibrational Effects on CT and PT.* There are several interesting points regarding the vibrational effects shown in Figure 9. Contrary to what we normally find, the largest effects come at high E_{col}, where E_{vib} is a negligible

fraction of the available energy. In this high E_{col} range the patterns of vibrational mode effects on all three channels are similar—those for CT and PT being nearly identical. ν_6^+, ν_4^+, and ν_5^+ slightly enhance both CT and PT at all collision energies, with enhancement ratios somewhat larger for PT, but still $<\sim$8%. The effects of ν_3^+ and ν_2^+ change with E_{col}, from slight enhancement at low E_{col} to significant inhibition at high E_{col}. The similarity in effects between CT and PT is surprising because these channels, both with large cross sections, clearly compete for product flux. For competing channels, vibrational mode effects are often anti-correlated;[29,40] i.e., a mode that enhances one major channel necessarily inhibits others. In $H_2CO^+ + ND_3$, vibration influences the total cross section, but inter-channel competition is controlled by some other factors, e.g., impact parameter and reactant orientation.

The largest vibrational effects occur in the high E_{col} range where CT is clearly dominated by a long-range electron hopping mechanism. As discussed above, efficient CT in a long-range mechanism is expected to require the existence of product states nearly resonant, and having good Franck−Condon overlap with the reactant state. In the CT process for $H_2CO^+ + ND_3$, the H_2CO moiety undergoes little geometry change, thus we expect that the best Franck−Condon overlap for H_2CO^+ neutralization will tend to conserve the reactant vibrational state: $H_2CO^+(\nu^+) \rightarrow H_2CO(\nu)$. As a consequence, the H_2CO product is not expected to take up much of the 0.72 eV of CT exoergicity. In contrast, ND_3 goes from pyramidal to planar upon ionization, favoring production of ND_3^+ with substantial excitation in ν_2^+, the umbrella bend. The Franck−Condon factors for the $ND_3 \rightarrow ND_3^+$ transition have been calculated by Ebata et al.[41] and can also be estimated from the photoelectron spectrum.[42] Assuming that all the 0.72 eV of CT exoergicity goes into ν_2^+, and using vibrational spacings measured in the photoelectron spectrum, production of ND_3^+ $\nu_2^+ = \sim 8$ would be required. The Franck−Condon factors coupling ground-state ND_3 with ND_3^+ are broadly peaked at $\nu_2^+ = \sim 6$, with the Franck−Condon factor for $\nu_2^+ = 8$ only ~10% below the peak value. The large CT cross section can, therefore, be rationalized in terms of high efficiency for transitions like: $H_2CO^+(\nu^+) + ND_3 \rightarrow H_2CO(\nu) + ND_3^+$ ($\nu_2^+ = \sim 8$).

It seems reasonable to assume that the effects of H_2CO^+ ν_2^+ and ν_3^+ vibrations on CT must involve degradation of the Franck−Condon or resonance conditions for efficient CT. As noted, there is little geometry change in the neutralization. Of course, Franck−Condon factors depend not only on the equilibrium geometries, but also on the shape of the potential well. Comparison of normal coordinates calculated for H_2CO^+ and H_2CO provide a measure of how the potential changes. At both B3LYP/6-311++G** and MP2/6-311++G** levels of theory, the normal coordinates are essentially unchanged upon neutralization, for all modes except ν_2 (nominally the CO stretch) and ν_3 (nominally the CH_2 scissors bend) which undergo significant Duschinsky rotation. For example, in the cation, the ν_3^+ mode is characterized as almost pure CH_2 scissors bending; i.e., the CH_2 bending amplitude is nearly 25 times larger than the amplitude of CO bond extension in the normal coordinate. In neutral H_2CO, the ratio of CH_2 bending and CO extension amplitudes is only 5. Similarly, for ν_2 in the cation, the CO stretching amplitude is ~5 times the amplitude of CH_2 scissor bending, whereas in neutral H_2CO, the CO stretch amplitude is only twice the bending amplitude. This mode mixing is a signature of changes in the potential along the CO stretching and CH_2 scissors coordinates, which should change the Franck−Condon factors.

Approximate Franck−Condon factors for H_2CO^+ neutralization were calculated within the independent harmonic oscillator, normal mode approximation, using the Sharp−Rosenstock−Chen algorithm[43,44] evaluated by the program PESCAL.[45,46] As suggested by the normal coordinate analysis, the Franck−Condon factors are essentially unity (>0.97) for the diagonal transitions in all modes except ν_2 and ν_3, where the diagonal Franck−Condon factors are 0.88 and 0.79, respectively. Given the approximations used in calculating the Franck−Condon factors, this analysis is only semiquantitative. Nonetheless, it seems reasonable to attribute the vibrational inhibition from ν_2^+ and ν_3^+ to diminished Franck−Condon overlaps for the energetically favorable transitions, requiring closer reactant approach before CT becomes efficient.

The question remains: Why are the vibrational effects for PT so similar to those for CT. As outlined above, CT occurs at a range large enough that it probably also occurs during reactant approach in collisions that ultimately give PT products. The vibrational effects indicate that inhibiting CT somehow also inhibits PT. A possible explanation would be if formation of the PT products were much more efficient in the $ND_3^+ + H_2CO$ charge state than in the reactant charge state (i.e., if PT were really CT followed by H atom transfer). Such a mechanism would lead to the observed 1:1 correlation of CT and PT vibrational effects; however, there are several problems. If CT is really necessary to generate PT products, we might expect that PT should be inefficient for the $H_2CO^+ + D_2O$ system, where CT is energetically inaccessible. In fact, PT(D_2O) occurs with unit efficiency. Furthermore, the ~20−30% ν_2^+ and ν_3^+ inhibition of σ_{CT} only corresponds to a 10−15% decrease in the distance where CT becomes efficient (R_{CT}). R_{CT} is still considerably larger than $R_{HardSphere}$, however; thus CT still can occur during reactant approach in collisions at $b < b_{HardSphere}$.

Another idea is akin to the harpooning mechanism developed to account for the large cross sections for collision of alkali atoms with halogens.[27] In the archetypal harpooning process, a long-range CT event takes place, switching the system from the weakly attractive neutral potential to a strongly attractive ion-pair potential, which is the ground state at short inter-reactant separations. The result is a large increase in the cross section for subsequent reaction. For ion−molecule systems, CT only switches from one ion−molecule potential to another; however, the effect may still be significant. The ion-induced-dipole and ion−dipole potentials responsible for the long-range attractive potential are determined by the polarizability and dipole moment of the neutral reactant. The polarizability and dipole moment of ND_3 are 2.22 Å^3 and 1.47 D, respectively, compared to 2.8 Å^3 and 2.33 D for H_2CO. As a consequence, the long-range attractive potential strengthens by ~50% when the charge is transferred. The idea is that if CT occurs at long range, the net attraction experienced during reactant approach is larger than if CT occurs at shorter separations, and therefore larger impact parameters may lead to atom transfer reactions. To estimate the significance of this effect, we ran a series of classical trajectories, with the potential treated as the sum of ion-induced-dipole and ion−dipole potentials, as above, but with polarizability and dipole moment switched to simulate CT during reactant approach. We looked for the maximum impact parameter that reached separations $\leq R_{HardSphere}$ (2.8 Å), where PT is assumed to be possible. For $E_{col} = 2.1$ eV, and allowing CT at 4.1 Å reactant separation (R_{CT} for ground-state H_2CO^+, see above), b_{max} is 3.2 Å. When R_{CT} is decreased to simulate the ~30% reduction in σ_{CT} upon ν_2^+ excitation, b_{max} decreases to 3.15 Å, corresponding to a decrease in cross section of ~3%, far smaller

than 20% inhibition observed for σ_{PT}. For reference, if CT is not allowed at all, then b_{max} is 3.1 Å, i.e., ~6.5% smaller than when CT is allowed to occur at 4.1 Å. We conclude that, though this potential switching mechanism probably contributes to the correlation of CT and PT vibrational effects, it probably cannot account for the strength of the correlation. Some other effect, at present unknown, couples these two channels.

(2) Vibrational Effects on the HA Threshold. Figure 8 shows the E_{col} and H_2CO^+ vibrational state dependence of σ_{HA}. An obvious question is how vibration compares to E_{col} in driving the endoergic HA reaction, either by contributing to the energy required, or by affecting the competition with the major PT and CT products. Vibrational effects at high energies are determined by the *average* effect of vibration on reactivity and appear to be grossly similar to those for PT and CT, as discussed above. Vibrational effects on the threshold energy, itself, are a measure of whether there are *any* collisions that are able to utilize the vibrational energy in overcoming the endoergicity. The thermodynamic threshold for the HA reaction is 0.13 eV, and at our lowest nominal E_{col} (~0.1 eV), the experimental collision energy spread is large enough that the cross section is already nonzero. Ordinarily, we would fit the E_{col} dependence of the cross sections to extract thresholds, corrected for the broadening; however, because this is such a small cross section, the uncertainty in the extracted threshold energies is high. We, therefore, merely note that the fitted ground-state threshold is consistent with the thermodynamics; i.e., there is no barrier in excess of the endoergicity.

It is obvious from the raw cross sections that E_{vib} is considerably less effective than E_{col} in the driving reaction near the threshold. For example, the highest energy mode, ν_5^+, has $E_{vib} = 0.337$ eV. An increase of 0.337 eV in E_{col} in the near-threshold region increases σ_{HA} by roughly a factor of 6 (averaging the effects for the two lowest energy points to reduce the uncertainty), whereas adding a quantum of ν_5^+ increases σ_{HA} by a factor of only ~1.7 for the same two E_{col} points. On this measure, E_{vib} is about one-third as effective as E_{col}. Similarly, if we crudely extrapolate the cross sections to estimate appearance energies (AEs), the shift in AE resulting from ν_5^+ excitation is ~100 meV, again indicating that E_{vib} is roughly one-third as effective as E_{col}. With the possible exception of ν_4^+, the lower frequency modes are also less effective than E_{col}, although the small energies involved make it difficult to estimate by what factors. Note, for example, that the second highest frequency mode, ν_2^+ (CO stretch), appears to be completely ineffective in shifting the threshold to lower E_{col}. The collision energy range near 0.5 eV is transitional between the enhancements near threshold, and the inhibitions observed at high energies. In this E_{col} range, only ν_5^+ and ν_4^+ continue to enhance HA. Continued enhancement of this endoergic channel by ν_5^+, the highest energy mode, is not surprising; however, ν_4^+ is one of the lower frequency modes, and the enhancement presumably has something to do with the out-of-plane bend motion being excited. We note that the calculated low energy pathway to HA products (Figure 2) involves formation of complex C, and then transition over TS(C−E). In both these structures, the H_2CO moiety is strongly out-of-plane bent; thus it is not unreasonable that excitation of the ν_4^+ mode might significantly enhance the probability of traversing this pathway to HA products.

That the vibrational effects on the threshold are weak and mode-specific, is somewhat surprising. In fitting thresholds to extract thermochemistry, it is usually assumed[47] that E_{vib} and E_{col} are equally effective at threshold. We have found several cases where this is true,[10,48] but others where vibration is ineffective[49] or has weak or mode-specific effects.[8,50] In the above threshold range, every system we have examined has vibrational effects that are substantially different than those of E_{col}—sometimes enhancing, sometimes inhibiting.

Acknowledgment. We thank Prof. Tomas Baer for helpful advice and discussions, both specific and general, over the past 25 years. We gratefully acknowledge Kent Ervin for assisting us with using his PESCAL and FCFGAUS program for Franck-Condon factor calculations. This work was supported by the National Science Foundation under Grant No. CHE-0110318.

References and Notes

(1) Dalgarno, A.; Black, J. H. *Rep. Prog. Phys.* **1976**, *39*, 573.
(2) Amin, M. Y.; El Nawawy, M. S.; Ateya, B. G.; Aiad, A. *Earth, Moon, Planets* **1995**, *69*, 127.
(3) Huntress, W. T., Jr. *Astrophys. J., Suppl. Ser.* **1977**, *33*, 495.
(4) Karpas, Z.; Anicich, V. G.; Huntress, W. T., Jr. *Chem. Phys. Lett.* **1978**, *59*, 84.
(5) Smith, D.; Adams, N. G. *Astrophys. J.* **1977**, *217*, 741.
(6) Adams, N. G.; Smith, D.; Grief, D. *Int. J. Mass Spectrom. Ion Phys.* **1978**, *26*, 405.
(7) Chiu, Y.-H.; Fu, H.; Huang, J.-T.; Anderson, S. L. *J. Chem. Phys.* **1995**, *102*, 1199.
(8) Chiu, Y.-H.; Fu, H.; Huang, J.-T.; Anderson, S. L. *J. Chem. Phys.* **1996**, *105*, 3089.
(9) Chiu, Y.-H. Reactant state-selection and product energy disposal in polyatomic ion−molecule reactions. Ph.D., State University of New York at Stony Brook, 1996.
(10) Liu, J.; Van Devener, B.; Anderson, S. L. *J. Chem. Phys.* **2002**, *116*, 5530.
(11) Spence, R.; Wild, W. *J. Chem. Soc.* **1935**, 338.
(12) Dainton, F. S.; Ivin, K. J.; Walmsley, D. A. G. *Trans. Farady Soc.* **1959**, *55*, 61.
(13) Liu, J.; Kim, H.-T.; Anderson, S. L. *J. Chem. Phys.* **2001**, *114*, 9797.
(14) Gerlich, D. *Adv. Chem. Phys.* **1992**, *82*, 1.
(15) Frisch, M. J.; Trucks, G. W.; Schlegel, H. B.; Scuseria, G. E.; Robb, M. A.; Cheeseman, J. R.; Montgomery, J. A., Jr.; Vreven, T.; Kudin, K. N.; Burant, J. C.; Millam, J. M.; Iyengar, S. S.; Tomasi, J.; Barone, V.; Mennucci, B.; Cossi, M.; Scalmani, G.; Rega, N.; Petersson, G. A.; Nakatsuji, H.; Hada, M.; Ehara, M.; Toyota, K.; Fukuda, R.; Hasegawa, J.; Ishida, M.; Nakajima, T.; Honda, Y.; Kitao, O.; Nakai, H.; Klene, M.; Li, X.; Knox, J. E.; Hratchian, H. P.; Cross, J. B.; Adamo, C.; Jaramillo, J.; Gomperts, R.; Stratmann, R. E.; Yazyev, O.; Austin, A. J.; Cammi, R.; Pomelli, C.; Ochterski, J. W.; Ayala, P. Y.; Morokuma, K.; Voth, G. A.; Salvador, P.; Dannenberg, J. J.; Zakrzewski, V. G.; Dapprich, S.; Daniels, A. D.; Strain, M. C.; Farkas, O.; Malick, D. K.; Rabuck, A. D.; Raghavachari, K.; Foresman, J. B.; Ortiz, J. V.; Cui, Q.; Baboul, A. G.; Clifford, S.; Cioslowski, J.; Stefanov, B. B.; Liu, G.; Liashenko, A.; Piskorz, P.; Komaromi, I.; Martin, R. L.; Fox, D. J.; Keith, T.; Al-Laham, M. A.; Peng, C. Y.; Nanayakkara, A.; Challacombe, M.; Gill, P. M. W.; Johnson, B.; Chen, W.; Wong, M. W.; Gonzalez, C.; Pople, J. A. *Gaussian 03*, revision B.02; Gaussian, Inc.: Pittsburgh, PA, 2003.
(16) Foresman, J. B.; Frisch, A. *Exploring Chemistry with Electronic Structure Methods*, 2nd ed.; Gaussian: Pittsburgh, 1993.
(17) Zhu, L.; Hase, W. L. *Quantum Chem. Prog. Exchange*, *QCPE 644*.
(18) Lias, S. G.; Bartmess, J. E.; Liebman, J. F.; Holmes, J. L.; Levin, R. D.; Mallard, W. G. *J. Phys. Chem. Ref. Data* **1988**, *17*, 1.
(19) Lias, S. G, in *NIST Standard Reference Database Number 69*; Linstrom, P. J., Mallard, W. G., Eds.; National Institute of Standards and Technology: Gaithersburg, MD, 2003; http://webbook.nist.gov.
(20) Ikezoe, Y.; Matsuoka, S.; Takebe, M.; Viggiano, A. *Gas-phase ion−molecule reaction rate constants through 1986.*; Mass Spec. Soc. of Japan: Tokyo, 1987.
(21) Troe, J. *Chem. Phys. Lett.* **1985**, *122*, 425.
(22) Coitino, E. L.; Lledos, A.; Serra, R.; Bertran, J.; Ventura, O. N. *J. Am. Chem. Soc.* **1993**, *115*, 9121.
(23) Bouma, W. J.; Nobes, R. H.; Radom, L. *Org. Mass Spectrom.* **1982**, *17*, 315.
(24) Curtiss, L. A.; Kock, L. D.; Pople, J. A. *J. Chem. Phys.* **1991**, *96*, 4040.
(25) Burgers, P. C.; Lifshitz, C.; Ruttink, P. J. A.; Schaftenaar, G.; Terlouw, J. K. *Org. Mass Spectrom.* **1989**, *24*, 579.
(26) Coitino, E. L.; Pereira, A.; Ventura, O. N. *J. Chem. Phys.* **1995**, *102*, 2833.
(27) Levine, R. D.; Bernstein, R. B. *Molecular Reaction Dynamics and Chemical Reactivity*; Oxford University Press: New York, 1987.

(28) Fisk, G. A.; McDonald, J. D.; Herschbach, D. R. *Discuss. Faraday Soc.* **1967**, *44*, 228.

(29) Kim, H.-T.; Liu, J.; Anderson, S. L. *J. Chem. Phys.* **2001**, *115*, 5843.

(30) Laudenslager, J. B.; Huntress, W. T., Jr.; Bowers, M. T. *J. Chem. Phys.* **1974**, *61*, 4600.

(31) Su, T.; Bowers, M. T. Classical ion−molecule collision theory. In *Gas-Phase Ion Chemistry*; Bowers, M. T., Eds.; Academic Press: New York, 1979; Vol. 1, p 84.

(32) Hase, W. L.; Bolton, K.; de Sainte Claire, P.; et al. VENUS99: A general chemical dynamics computer program, 1999.

(33) Rodgers, M. T.; Ervin, K. M.; Armentrout, P. B. *J. Chem. Phys.* **1997**, *106*, 4499.

(34) Bueker, H.-H.; Uggerud, E. *J. Phys. Chem.* **1995**, *99*, 5945.

(35) Bueker, H.-H.; Helgaker, T.; Ruud, K.; Uggerud, E. *J. Phys. Chem.* **1996**, *100*, 15388.

(36) Cheng, H. *J. Chem. Phys. 105*, 6844.

(37) Li, Y.; Farrar, J. M. *J. Chem. Phys.* **2004**, *120*, 199.

(38) Liu, J.; Devener, B. V.; Anderson, S. L. *J. Chem. Phys.* **2003**, *119*, 200.

(39) Liu, J.; Song, K.; Hase, W. L.; Anderson, S. L. *J. Am. Chem. Soc.* **2004**, *126*, 8602.

(40) Morrison, R. J.; Conaway, W. E.; Ebata, T.; Zare, R. N. *J. Chem. Phys.* **1986**, *84*, 5527.

(41) Ebata, T.; Conaway, W. E.; Zare, R. N. *Int. J. Mass Spectrom. Ion Processes* **1987**, *80*, 51.

(42) Weiss, M. J.; Lawrence, G. M. *J. Chem. Phys.* **1970**, *53*, 214.

(43) Sharp, T. E.; Rosenstock, H. M. *J. Chem. Phys.* **1964**, *41*, 3453.

(44) Chen, P. Photoelectron spectroscopy of reactive intermediates. In *Unimolecular and bimolecular ion−molecule reaction dynamics*; Ng, C. Y., Baer, T., Powis, I., Eds.; John Wiley & Sons Ltd: New York, 1994; p371.

(45) Ervin, K. M.; Ramond, T. M.; Davico, G. E.; Schwartz, R. L.; Casey, S. M.; Lineberger, W. C. *J. Phys. Chem. A* **2001**, *105*, 10822.

(46) Ervin, K. M. PESCAL, Fortran program, 2003.

(47) Armentrout, P. B. *Int. J. Mass Spectrom.* **2000**, *200*, 219.

(48) Yang, B.; Chiu, Y. H.; Fu, H.; Anderson, S. L. *J. Chem. Phys.* **1991**, *95*, 3275.

(49) Liu, J.; Anderson, S. L. *J. Chem. Phys.* **2004**, *120*, 8528.

(50) Liu, J.; Devener, B. V.; Anderson, S. L. *J. Chem. Phys.* **2002**, *117*, 8292.